


Robust spin-valley polarization in commensurate MoS₂/graphene heterostructuresLuojun Du,^{1,2} Qian Zhang,¹ Benchao Gong,¹ Mengzhou Liao,² Jianqi Zhu,² Hua Yu,² Rui He,³ Kai Liu,¹ Rong Yang,² Dongxia Shi,^{2,4} Lin Gu,^{2,5} Feng Yan,⁶ Guangyu Zhang,^{2,4,5,*} and Qingming Zhang^{1,7,†}¹*Department of Physics, Beijing Key Laboratory of Opto-Electronic Functional Materials and Micro-nano Devices, Renmin University of China, Beijing 100872, China*²*Beijing National Laboratory for Condensed Matter Physics and Institute of Physics, Chinese Academy of Sciences, Beijing 100190, China*³*Department of Electrical and Computer Engineering, Texas Tech University, Lubbock, Texas 79409, USA*⁴*School of Physical Sciences, University of Chinese Academy of Science, Beijing 100190, China*⁵*Collaborative Innovation Center of Quantum Matter, Beijing 100190, China*⁶*Department of Applied Physics, The Hong Kong Polytechnic University, Hung Hom, 999077, Kowloon, Hong Kong*⁷*Department of Physics and Astronomy, Shanghai Jiao Tong University, Shanghai 200240 and Collaborative Innovation Center of Advanced Microstructures, Nanjing 210093, China* (Received 13 August 2017; revised manuscript received 14 November 2017; published 27 March 2018)

The investigation and control of quantum degrees of freedom (DoFs) of carriers lie at the heart of condensed-matter physics and next-generation electronics/optoelectronics. van der Waals heterostructures stacked from distinct two-dimensional (2D) crystals offer an unprecedented platform for combining the superior properties of individual 2D materials and manipulating spin, layer, and valley DoFs. MoS₂/graphene heterostructures, harboring prominent spin-transport properties of graphene, giant spin-orbit coupling, and spin-valley polarization of MoS₂, are predicted as a perfect venue for optospintronics. Here, we report the epitaxial growth of commensurate MoS₂ on graphene with high quality by chemical vapor deposition, and demonstrate robust temperature-independent spin-valley polarization at off-resonant excitation. We further show that the helicity of *B* exciton is larger than that of *A* exciton, allowing the manipulation of spin bits in the commensurate heterostructures by both optical helicity and wavelength. Our results open a window for controlling spin DoF by light and pave a way for taking spin qubits as information carriers in the next-generation valley-controlled optospintronics.

DOI: [10.1103/PhysRevB.97.115445](https://doi.org/10.1103/PhysRevB.97.115445)

Graphene is an exotic spintronics candidate featuring Dirac fermions, two inequivalent valleys [1], ultrahigh electron mobility, room-temperature ballistic transport [2], and long spin-relaxation lengths and times [3–6]. However, electric-field modulation of spin degrees of freedom (DoFs) in graphene is almost impossible due to a tiny intrinsic spin-orbit coupling (SOC) ($\sim 10 \mu\text{eV}$) [7]. In contrast, monolayer transition-metal dichalcogenides (*MX*₂), in which the chalcogen atoms in two hexagonal planes are separated by a single layer of metal atoms in a trigonal prismatic structure, have a strong SOC resulting from *d* orbitals of heavy metal atoms, and inversion symmetry breaking [8]. In combination with time-reversal symmetry, the spin and valley DoFs are inherently entangled [9] and carriers in different valleys are associated with contrasted Berry curvature and magnetic moment, allowing the excitation of spin- and valley-polarized carriers by circularly polarized light [10–12]. Therefore, monolayer *MX*₂ is an ideal material integrating both valleytronics and spintronics. On the other hand, unavoidable defects and low mobility of carriers ($\mu < 100 \text{ cm}^2 \text{ V}^{-1} \text{ s}^{-1}$) in monolayer *MX*₂ are critical barriers to the application and development of spintronics and valleytronics [13].

*MX*₂/graphene heterostructures with weak van der Waals coupling offer a playground to combine these excellent performances of both graphene and *MX*₂, including ultrahigh mobility, micrometer-scale spin-transport lengths [14], and nanosecond-scale spin-relaxation times [15] in graphene and strong SOC [8], coupled spin and valley [9], and valley-selective circular dichroism [10] in monolayer *MX*₂. Recent experiments have demonstrated strong proximity SOC acquired by graphene [16–18] and ultrafast charge transfer [19] in *MX*₂/graphene heterostructures. And, the *MX*₂/graphene heterostructures have been theoretically proven to be promising for novel optospintronics, because spin-polarized carriers can be nicely provided by *MX*₂ and optically injected into graphene with spin *S*_z as a good quantum number [20]. Moreover, Luo *et al.* recently demonstrated the spin injection and opto-valleytronic spin valves of MoS₂/graphene heterostructures produced by the transfer approach [21]. However, there are some disadvantages for those MoS₂/graphene heterostructures obtained by the transfer approach. For example, interlayer twisting angles are arbitrary and bubbles, wrinkles, and residuals at interface are always problematic. To the best of our knowledge, commensurate MoS₂/graphene heterostructures with cleaner interface and stronger interlayer coupling can be obtained via chemical vapor deposition (CVD) [22–24] and solve these problems perfectly. Thus, the commensurate MoS₂/graphene heterostructures are expected to be more suitable for optospintronics application.

*gyzhang@iphy.ac.cn

†qmzhang@ruc.edu.cn

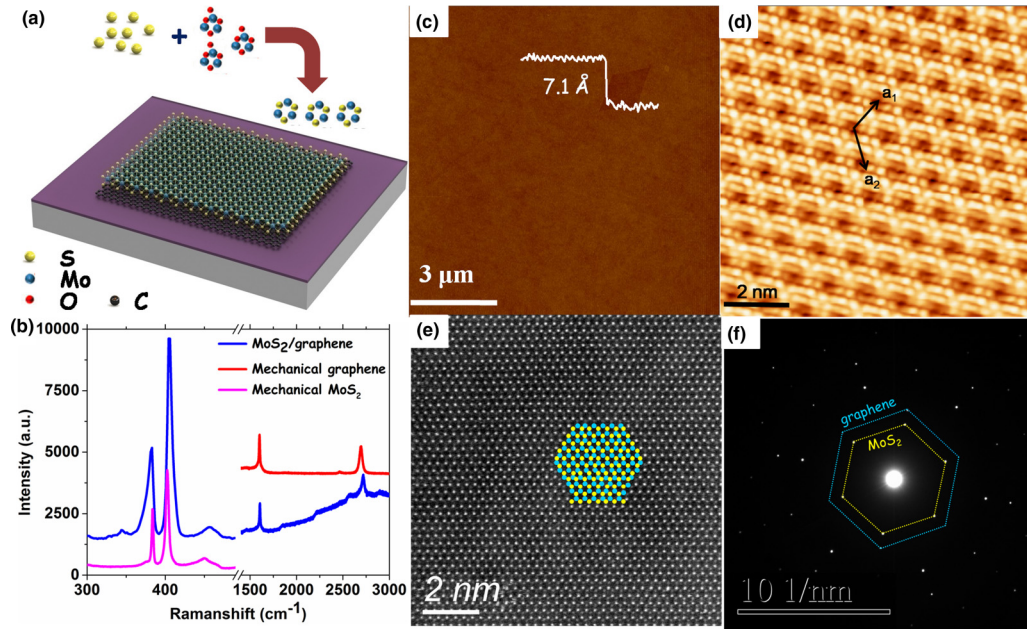


FIG. 1. (a) Schematic illustration of the growth process. Yellow, blue, red, and black balls represent sulfur, molybdenum, oxygen, and carbon atoms, respectively. (b) Raman spectra for MoS₂/graphene heterostructures (blue line), mechanically exfoliated MoS₂ (magenta line), and mechanically exfoliated graphene (red line) at 2.33-eV excitation. (c) AFM image of MoS₂/graphene heterostructures. A height profile was extracted along the white line. (d) STM topographic image showing 1.4-nm moiré patterns. (e) Atomic-resolution ADF-STEM image of suspended MoS₂/graphene heterostructures on a TEM grid. The brighter (dimmer) spots are molybdenum (sulfur) atoms. The hexagonal lattice shows alternate molybdenum and sulfur sites with the top-view schematics overlaid. (f) SAED pattern of MoS₂/graphene heterostructures.

In this article, we performed polarization-resolved photoluminescence (PL) on commensurate MoS₂/graphene heterostructures obtained by van der Waals epitaxial growth. It is experimentally demonstrated that contrasting spin polarization could be generated in the commensurate MoS₂/graphene heterostructures by not only distinct optical polarization but also the same helicity at different excitation energy. In addition, temperature-dependent measurements show that the valley-controlled spin polarization is almost independent of temperature and can persist up to room temperature. In combination with our theoretical calculation that the SOC in graphene is strongly enhanced, our commensurate MoS₂/graphene heterostructures are candidates for realizing optospintronics.

MoS₂/graphene heterostructures, prototypical MX₂/graphene heterostructures, were fabricated via epitaxial growth of MoS₂ on graphene through an oxygen-assisted CVD process [24] (more details in Supplemental Material, section S1 [25]). A schematic of the epitaxial growth process is demonstrated in Fig. 1(a), illustrating the formation of MoS₂ on graphene by MoO₃ reacting with S. As-grown MoS₂/graphene heterostructures were characterized by Raman spectroscopy [Fig. 1(b)]. We can see some prominent features in the spectrum, such as the first-order E' (~ 382 cm⁻¹) and A'_1 (~ 404 cm⁻¹) modes of MoS₂, G band (~ 1600 cm⁻¹), and $2D$ band (~ 2710 cm⁻¹) of graphene, and a broad background at high wave number associated with the PL of MoS₂. As compared with mechanically exfoliated MoS₂ and graphene, the frequency difference between E' and A'_1 modes increases, and both G and $2D$ peaks blue shift in MoS₂/graphene heterostructures, indicating a strong interlayer coupling (Supplemental Material, section S1 [25]) [26,27].

The asymmetric and broad E' mode in the MoS₂/graphene heterostructures evidences the lattice strain in MoS₂. This is in harmony with our recent work [24], demonstrating that commensurate MoS₂/graphene heterostructures possess the largest strain for all the twisting angles, and strain for commensurate MoS₂/graphene heterostructures is about 0.3% larger than that for MoS₂/graphene heterostructures at twisting angle = 30°. An atomic force microscopy (AFM) image [Fig. 1(c)] reveals the thickness of 7.1 Å for MoS₂, in agreement with monolayer level. An atomic-resolution AFM lateral image (Supplemental Material, section S1 [25]) clearly shows the hexagonal lattice of the higher-lying S atoms, and the periods of atomic corrugation of 3.18 Å, corresponding to the in-plane S–S distance.

MoS₂/graphene heterostructures, akin to graphene/boron nitride heterostructures or twisted graphene layers [28,29], exhibit a rotation-dependent topographic moiré pattern, determined by the lattice mismatch and relative rotation angle between MoS₂ and graphene (Supplemental Material, section S2 [25]). A scanning tunneling microscopy (STM) topographic image [Fig. 1(d)] shows the distinct moiré pattern of MoS₂/graphene heterostructures with moiré wavelength of 1.4 nm, indicating the van der Waals commensurate epitaxial growth and zero twisting angle between MoS₂ and graphene (Supplemental Material, Fig. S3 [25]).

With the aberration-corrected annular dark-field scanning transmission electron microscopy (ADF-STEM), the honeycomb lattice structures of MoS₂ with two sublattice sites occupied by one molybdenum (brighter spots) and two stacked sulfur atoms (dimmer spots) are clearly visible, as illustrated by the top-view schematics [Fig. 1(e)]. The MoS₂ layer

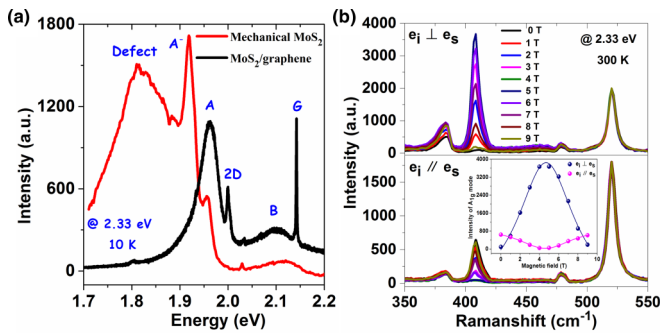


FIG. 2. (a) Photoluminescence spectrum for MoS₂/graphene heterostructures (black) and mechanically exfoliated MoS₂ (red) at 2.33-eV excitation and 10 K. (b) Polarized Raman spectra for MoS₂/graphene heterostructures at room temperature with applied magnetic field and in the cross-polarized (upper) configuration (incident light polarization e_i and scattered light polarization e_s are perpendicular to each), and copolarized (lower) configuration (e_i and e_s are parallel to each). Inset: magnetic-field dependence of the A_1' mode intensity for MoS₂/graphene heterostructures.

displays a perfect hexagonal atomic structure with low number of vacancies and topological defects, being consistent with the high quality for van der Waals epitaxial growth [30] and confirmed by our optical results (see below). Selected-area electron diffraction (SAED) pattern [Fig. 1(f)] reveals that two sets of sixfold symmetry diffraction spots, originated from MoS₂ and graphene, respectively, are of the same orientation, in line with the moiré pattern of the STM topographic image.

We measured the PL spectrum at 10 K [Fig. 2(a)] and the magneto-optical Raman effect at room temperature [Fig. 2(b)] of the commensurate MoS₂/graphene heterostructures to further examine their quality. The emission spectrum for mechanically exfoliated MoS₂ was found to contain four features: (1) the strong emission around 1.92 eV contributed by neutral exciton A and negatively charged exciton (trion) A^- , with trion binding energy of 38 meV [10,31]; (2) the weak feature from B exciton (~ 2.1 eV), arising from SOC (158 meV) in the valence band; and (3) a broad feature near 1.8 eV, originated from emission of the defect-trapped exciton [10]. On the other hand, there are some distinct features in the PL spectrum of the commensurate MoS₂/graphene heterostructures: (1) A and B excitons from MoS₂, associated with direct optical transitions from the lowest conduction band to the highest spin-split valence band, and (2) G and $2D$ bands, arising from lattice vibrations of graphene. The full width at half maximum (FWHM) of the A exciton at 10 K is 42 and 48 meV for the commensurate MoS₂/graphene heterostructures and exfoliated MoS₂, respectively. The absence of both defect-trapped exciton and trion in the commensurate MoS₂/graphene heterostructures is strong evidence for a more homogeneous charge distribution with no unintentional doping and higher quality of the commensurate heterostructures.

Figure 2(b) presents the magnetic-field-dependent polarized Raman spectra of the commensurate MoS₂/graphene heterostructures with two scattering configurations: copolarized ($e_i \parallel e_s$) and cross polarized ($e_i \perp e_s$). The E' mode of MoS₂ and 521-cm⁻¹ mode of Si substrate are almost magnetic-

field-independent (Supplemental Material, section S3 [25]). In contrast, the A_1' mode of MoS₂ displays a gigantic anti-correlated Raman intensity modulation with magnetic field in the two orthogonal polarization configurations [Fig. 2(b), inset], revealing that the commensurate MoS₂/graphene heterostructures favor fascinating magnetically tunable Raman effect and magneto-optical applications. This magneto-optical Raman effect stems from magnetic-field-induced horizontal twofold symmetry breaking and has been carefully studied in mechanically exfoliated MoS₂ [32]. The resonance magnetic-field strength at which the phonon intensity achieves its extremum (maximum or minimum) is inversely proportional to optical mobility and hence a good index of intrinsic electronic scattering. The resonance magnetic field obtained by fitting the field dependence of Raman intensities to the functions given in Ref. [32] is at 4.66 T [Fig. 2(b), inset] in the commensurate MoS₂/graphene heterostructures, less than the value (~ 6 T) in mechanically exfoliated MoS₂ [32], reflecting that the commensurate MoS₂/graphene heterostructures enjoys higher intrinsic optical mobility and carriers suffer less scattering. This result is in good harmony with the PL spectrum, STEM, and STM topographic images of the heterostructures.

Chiral interband transitions are exactly at two valleys (left circularly polarized σ_- and right circularly polarized σ_+ at K and K' valleys, respectively) and can evolve to excitons as a result of lattice structures and time-reversal symmetry [Fig. 3(c)]. The helicity polarized PL spectra at 10 K, excited by σ_- radiation on resonance with the A exciton at 1.96 eV, are presented in Figs. 3(d) (mechanically exfoliated MoS₂) and 3(e) (commensurate MoS₂/graphene heterostructures). Following the convention used in Ref. [10], the degree of valley-spin polarization is defined as the helicity: $\rho = \frac{I(\sigma_-) - I(\sigma_+)}{I(\sigma_-) + I(\sigma_+)}$, where $I(\sigma_-)/I(\sigma_+)$ is the intensity of the left/right-handed circular component. The valley-spin polarization of mechanically exfoliated MoS₂ drops dramatically with increasing temperatures and almost disappears above 240 K [Fig. 3(f)], in line with Refs. [10,11]. In sharp contrast, the helicity of commensurate MoS₂/graphene heterostructures exhibits a rather slow decay tendency and holds valley-spin polarization (~ 0.26) at room temperature [Fig. 3(f)]. The helicity of commensurate MoS₂/graphene heterostructures at low temperatures is found to be lower than that of the exfoliated MoS₂. It may be ascribed to the strain induced by the immense lattice mismatch and van der Waals interaction between MoS₂ and graphene [33,34]. The polarization-resolved PL spectrum under σ_- excitation off resonance (2.33 eV) with excitons are also measured for mechanically exfoliated MoS₂ [Fig. 3(g)] and MoS₂/graphene heterostructures [Fig. 3(h)]. No polarization is observed for mechanically exfoliated MoS₂, while commensurate MoS₂/graphene heterostructures harbor valley-spin polarization that is almost temperature-independent for both A and B excitons [Fig. 3(i)]. More surprisingly, the helicity at 10 K for B exciton (~ 0.61) is much larger than that for A exciton (~ 0.22), being similar to anomalous spin-valley polarization in MoSe₂ [35]. The higher spin-valley polarization for B exciton may stem from the fact that the B exciton is closer to 2.33 eV. The finding indicates that we could generate opposite spin polarization by tuning not only circular polarization of incident light but also the excitation energies, because of opposite spins for A and B excitons [21,36]. This result is of particular

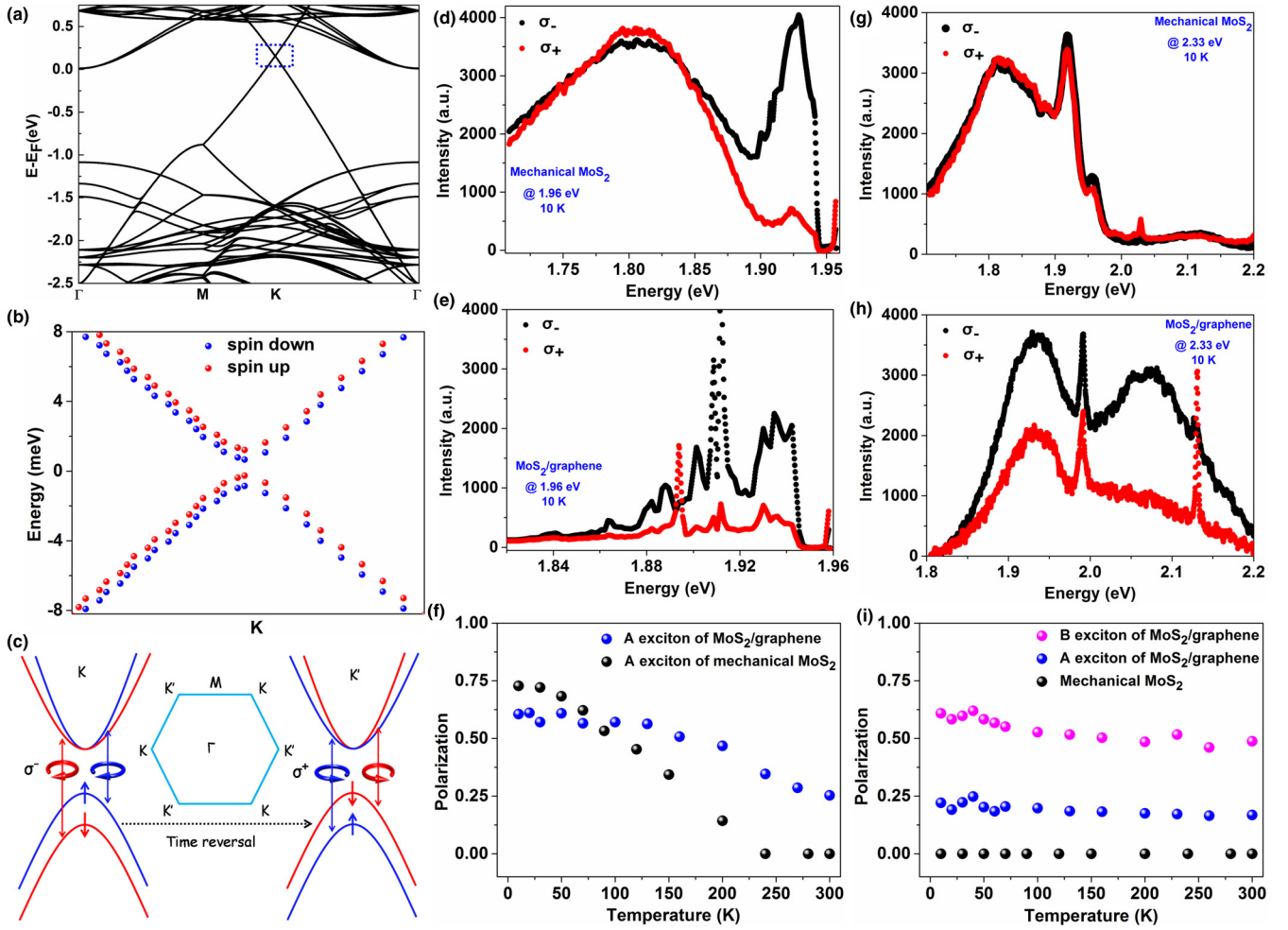


FIG. 3. All optical excitation is left circularly polarized (σ_-). (a) Electronic band structure of MoS₂/graphene heterostructures from DFT with SOC. (b) Zoom-in near the K valley [highlighted by the dashed box in (a)] shows graphene bands appearing gapped and spin-polarized due to proximity to MoS₂. The red (blue) bands are for spin-up (spin-down) states. (c) Schematics of valley-dependent optical selection rules and spin-valley locking at K/K' valleys in the momentum space of MoS₂. (d), (e) Polarization-resolved PL spectra of mechanically exfoliated MoS₂ (d) and MoS₂/graphene (e) versus photon energy for 1.96-eV excitation. (f) Degree of PL polarization as a function of temperature at 1.96-eV excitation. (g), (h) Polarization-resolved PL spectra of mechanically exfoliated MoS₂ (g) and MoS₂/graphene (h) versus photon energy for 2.33-eV excitation. (i) Degree of PL polarization versus temperature at 2.33-eV excitation.

significance for practical optospintronics applications, as will be seen below.

How to understand the robust spin-valley polarization of the commensurate MoS₂/graphene heterostructures? The helicity is determined by the steady-state spin-valley population (Supplemental Material, section S8 [25]), $\rho = \frac{N_K - N_{K'}}{N_K + N_{K'}} = \frac{1}{1 + 2\tau/\tau_S}$, where $\frac{1}{\tau}$ and $\frac{1}{\tau_S}$ denote the nonradiative decay rate (exciton lifetime) and the intervalley relaxation rate (valley lifetime), respectively. The radiative decay rate is not taken into account since it is assumed to be much lower than the nonradiative rate [10,12]. The exciton lifetime and valley lifetime for both the commensurate MoS₂/graphene heterostructures and mechanically exfoliated MoS₂ are almost identical since the degree of the spin-valley polarization of the commensurate MoS₂/graphene heterostructures at 10 K, excited by σ_- radiation at 1.96 eV, is akin to that of the mechanically exfoliated MoS₂ [Fig. 3(f)]. Thus, it should not be the major cause of robust spin-valley polarization in the commensurate MoS₂/graphene heterostructures.

Due to the spin-valley coupling in monolayer MoS₂, intervalley scattering is accompanied by spin-flipping, putting constraints on possible spin-scattering mechanisms related to the relaxation of spin-valley polarization. There are three main principal spin-relaxation channels in semiconductors: the Elliot-Yafet (EY) mechanism [37,38], the D'yakonov-Perel (DP) mechanism [39], and the Bir-Aronov-Pikus (BAP) mechanism [40]. In the DP mechanism, carriers with oriented spins experience a momentum-dependent internal magnetic field, leading to the spin Larmor process. Spin scattering through the DP mechanism is completely suppressed in monolayer MoS₂, because the exact 2D nature and mirror symmetry give zero value for in-plane component of internal magnetic field. The negligible effect of magnetic field on polarization also rules out the DP mechanism (Supplemental Material, section S7 [25]). Electron spin-flipping can occur via electron-hole exchange and annihilation interactions (BAP mechanism) as the electron-hole interaction is strongly enhanced by dielectric screening reduction in the 2D limit. However, the electron-hole

exchange in the commensurate MoS₂/graphene heterostructures and mechanically exfoliated MoS₂ has a similar scale and the BAP mechanism is unlikely to be the major factor for the robust spin-valley polarization in MoS₂/graphene heterostructures. The EY mechanism is attributed to the fact that Bloch electrons are not spin eigenstates in real crystals and spin-independent interaction with vacancies, grain boundaries, and phonons can lead to spin relaxation. A high density of sulfur vacancies in mechanically exfoliated MoS₂ cause the low mobility and PL quantum yield [13,41,42] and act as sharp magnetic scattering centers through exchange interactions between extra electrons and Mo⁴⁺ ions [43] to cause the effective relaxation. Spatial charge inhomogeneous distribution (coexistence of *A* and *A*⁻ excitons) in mechanically exfoliated MoS₂ can give rise to electron-hole puddles [44–46] and spin scattering. For the high-quality commensurate MoS₂/graphene heterostructures with homogeneous charge distributions and a low density of sulfur vacancies, the scattering is strongly suppressed. However, contribution of the exotic massless Dirac fermions in graphene to robust spin-valley polarization is not confirmed here. Further quantitative studies are needed to elaborate the mechanism.

Density-functional theory (DFT) calculations [Fig. 3(a)] reveal that the Dirac point of graphene is within the MoS₂ band gap and the lowest conduction band of MoS₂ is practically unchanged by the presence of graphene. Dirac fermions of graphene in the commensurate MoS₂/graphene heterostructures acquire meV-scale SOC [Fig. 3(b)] through the interfacial-induced global spin-orbit proximity effect, which is three orders of magnitude higher than the intrinsic value, making it possible to manipulate spin DoFs by electric field [16,20]. The manipulation of spin DoFs is the key for spintronics. In combination with robust spin-valley polarization, the high-quality commensurate MoS₂/graphene heterostructures become an exciting platform for optospintronics. Under 1.96-eV excitation on resonance with the *A* exciton, spin-up polarized (spin-down polarized) carriers can be manipulated by left (right) circularly polarized light. Since electron-hole pairs do not recombine immediately, the spin-polarized electron will inject into graphene from MoS₂ [19] and graphene harbors spin-up polarized (spin-down polarized) carriers, excited by left (right) polarized light. Using left circularly polarized light at 2.33-eV excitation, both *A* and *B* excitons of the *K* valley are excited. Since the spin states of *A* and *B* excitons are opposite and the spin-valley polarization of *B* exciton is much larger than that for *A* exciton [Fig. 3(i)], we can obtain the opposite spin-polarized carriers in graphene, as compared with

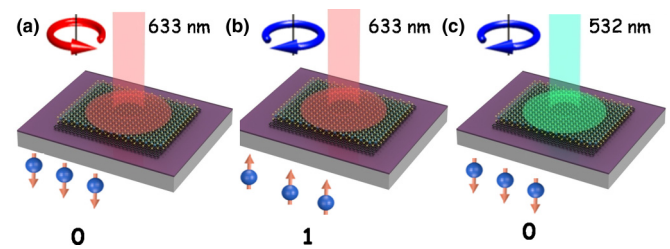


FIG. 4. (a), (c) Spin-down polarization and state 0 by right circularly polarized light at 633-nm excitation (a) and left circularly polarized light at 532-nm excitation (c). (b) Spin-up polarization and state 1 by left circularly polarized light at 633-nm excitation.

the same helicity at 633-nm excitation. This is in consistency with recent results based on MoS₂/graphene heterostructures produced by transfer approach [21]. We can define spin bits as follows: spin-up state as “1” and spin-down state as “0.” Thus, spin-up polarized (state 1) carriers can be manipulated by left circularly polarized light at 633-nm excitation [Fig. 4(b)], while we can obtain spin-down (state 0) polarized carriers by either right circularly polarized light at 633-nm excitation [Fig. 4(a)] or left circularly polarized light at 532-nm excitation [Fig. 4(c)]. The manipulation of spin bits in the commensurate MoS₂/graphene heterostructures through optical helicity and excitation energies enables intrinsic spin DoF for information processing and modern electronics.

In summary, high-quality commensurate MoS₂/graphene heterostructures have been obtained by van der Waals epitaxial growth, and anomalously robust spin-valley polarization is found in the commensurate heterostructures. The successful control of the spin DoF by both optical helicity and wavelength, and the gigantic spin-orbit coupling for Dirac fermions in the commensurate MoS₂/graphene heterostructures pave the way toward future optospintronic applications.

This research was support by the NSF of China (Grant No. 11474357) and the Ministry of Science and Technology of China (973 Project No. 2016YFA0300504), the National Basic Research Program of China (973 Program, Grants No. 2013CB934500 and No. 2013CBA01602), the Key Research Program of Frontier Sciences, CAS (Grant No. QYZDB-SSW-SLH004), the Strategic Priority Research Program (B) of the Chinese Academy of Sciences, CAS (Grant No. XDB07010100), and the National Science Foundation (NSF) of the U.S. (CAREER Grant No. DMR-1760668).

- [1] K. S. Novoselov, A. K. Geim, S. Morozov, D. Jiang, M. Katsnelson, I. Grigorieva, S. Dubonos, and A. A. Firsov, Two-dimensional gas of massless Dirac fermions in graphene, *Nature (London)* **438**, 197 (2005).
- [2] A. S. Mayorov, R. V. Gorbachev, S. V. Morozov, L. Britnell, R. Jalil, L. A. Ponomarenko, P. Blake, K. S. Novoselov, K. Watanabe, T. Taniguchi, and A. K. Geim, Micrometer-scale ballistic transport in encapsulated graphene at room temperature, *Nano Lett.* **11**, 2396 (2011).

- [3] N. Tombros, C. Jozsa, M. Popinciuc, H. T. Jonkman, and B. J. van Wees, Electronic spin transport and spin precession in single graphene layers at room temperature, *Nature* **448**, 571 (2007).
- [4] T. Maassen, J. J. van den Berg, N. IJbema, F. Fromm, T. Seyller, R. Yakimova, and B. J. van Wees, Long spin relaxation times in wafer scale epitaxial graphene on SiC (0001), *Nano Lett.* **12**, 1498 (2012).
- [5] M. Drögeler, C. Franzen, F. Volmer, T. Pohlmann, L. Banszerus, M. Wolter, K. Watanabe, T. Taniguchi, C. Stampfer, and

- B. Beschoten, Spin lifetimes exceeding 12 ns in graphene nonlocal spin valve devices, *Nano Lett.* **16**, 3533 (2016).
- [6] J. Ingla-Aynés, M. H. D. Guimarães, R. J. Meijerink, P. J. Zomer, and B. J. van Wees, 24- μm spin relaxation length in boron nitride encapsulated, *Phys. Rev. B* **92**, 201410 (2015).
- [7] S. Konschuh, M. Gmitra, and J. Fabian, Tight-binding theory of the spin-orbit coupling in graphene, *Phys. Rev. B* **82**, 245412 (2010).
- [8] Z. Zhu, Y. Cheng, and U. Schwingenschlögl, Giant spin-orbit-induced spin splitting in two-dimensional transition-metal dichalcogenide semiconductors, *Phys. Rev. B* **84**, 153402 (2011).
- [9] D. Xiao, G.-B. Liu, W. Feng, X. Xu, and W. Yao, Coupled Spin and Valley Physics in Monolayers of MoS_2 and other Group-VI Dichalcogenides, *Phys. Rev. Lett.* **108**, 196802 (2012).
- [10] K. F. Mak, K. He, J. Shan, and T. F. Heinz, Control of valley polarization in monolayer MoS_2 by optical helicity, *Nat. Nanotechnol.* **7**, 494 (2012).
- [11] H. Zeng, J. Dai, W. Yao, D. Xiao, and X. Cui, Valley polarization in MoS_2 monolayers by optical pumping, *Nat. Nanotechnol.* **7**, 490 (2012).
- [12] B. Zhu, H. Zeng, J. Dai, Z. Gong, and X. Cui, Anomalously robust valley polarization and valley coherence in bilayer WS_2 , *Proc. Natl. Acad. Sci. USA* **111**, 11606 (2014).
- [13] Z. Yu, Y. Pan, Y. Shen, Z. Wang, Z.-Y. Ong, T. Xu, R. Xin, L. Pan, B. Wang, L. Sun, J. Wang, G. Zhang, Y. W. Zhang, Y. Shi, and X. Wang, Towards intrinsic charge transport in monolayer molybdenum disulfide by defect and interface engineering, *Nat. Commun.* **5**, 5290 (2014).
- [14] P. Zomer, M. Guimaraes, N. Tombros, and B. Van Wees, Long-distance spin transport in high-mobility graphene on hexagonal boron nitride, *Phys. Rev. B* **86**, 161416 (2012).
- [15] T.-Y. Yang, J. Balakrishnan, F. Volmer, A. Avsar, M. Jaiswal, J. Samm, S. Ali, A. Pachoud, M. Zeng, M. Popinciuc, G. Güntherodt, B. Beschoten, and B. Özyilmaz, Observation of Long Spin-Relaxation Times in Bilayer Graphene at Room Temperature, *Phys. Rev. Lett.* **107**, 047206 (2011).
- [16] Z. Wang, D. K. Ki, H. Chen, H. Berger, A. H. MacDonald, and A. F. Morpurgo, Strong interface-induced spin-orbit interaction in graphene on WS_2 , *Nat. Commun.* **6**, 8339 (2015).
- [17] A. Avsar, J. Y. Tan, T. Taychatanapat, J. Balakrishnan, G. Koon, Y. Yeo, J. Lahiri, A. Carvalho, A. Rodin, E. O'Farrell, G. Eda, A. H. Castro Neto, and B. Özyilmaz, Spin-orbit proximity effect in graphene, *Nat. Commun.* **5**, 4875 (2014).
- [18] Z. Wang, D.-K. Ki, J. Y. Khoo, D. Mauro, H. Berger, L. S. Levitov, and A. F. Morpurgo, Origin and Magnitude of 'Designer' Spin-Orbit Interaction in Graphene on Semiconducting Transition Metal Dichalcogenides, *Phys. Rev. X* **6**, 041020 (2016).
- [19] J. He, N. Kumar, M. Z. Bellus, H.-Y. Chiu, D. He, Y. Wang, and H. Zhao, Electron transfer and coupling in graphene-tungsten disulfide van der Waals heterostructures, *Nat. Commun.* **5**, 5622 (2014).
- [20] M. Gmitra and J. Fabian, Graphene on transition-metal dichalcogenides: A platform for proximity spin-orbit physics and optospintronics, *Phys. Rev. B* **92**, 155403 (2015).
- [21] Y. K. Luo, J. Xu, T. Zhu, G. Wu, E. J. McCormick, W. Zhan, M. R. Neupane, and R. K. Kawakami, Opto-valleytronic spin injection in monolayer MoS_2 /few-layer graphene hybrid spin valves, *Nano Lett.* **17**, 3877 (2017).
- [22] Y.-C. Lin, N. Lu, N. Perea-Lopez, J. Li, Z. Lin, X. Peng, C. H. Lee, C. Sun, L. Calderin, P. N. Browning, M. S. Bresnahan, M. J. Kim, T. S. Mayer, M. Terrones, and J. A. Robinson, Direct synthesis of van der Waals solids, *ACS Nano* **8**, 3715 (2014).
- [23] G. W. Shim, K. Yoo, S.-B. Seo, J. Shin, D. Y. Jung, I.-S. Kang, C. W. Ahn, B. J. Cho, and S.-Y. Choi, Large-area single-layer MoSe_2 and its van der Waals heterostructures, *ACS Nano* **8**, 6655 (2014).
- [24] L. Du, H. Yu, M. Liao, S. Wang, L. Xie, X. Lu, J. Zhu, N. Li, C. Shen, P. Chen, R. Yang, D. Shi, and G. Zhang, Modulating PL and electronic structures of MoS_2 /graphene heterostructures via interlayer twisting angle, *Appl. Phys. Lett.* **111**, 263106 (2017).
- [25] See Supplemental Material at <http://link.aps.org/supplemental/10.1103/PhysRevB.97.115445> for details of oxygen-assisted CVD method, magneto-optical Raman effect, polarization-resolved PL spectra, and DFT calculation. This includes Refs. [20,28,34,47–53].
- [26] H. Ago, H. Endo, P. Solís-Fernández, R. Takizawa, Y. Ohta, Y. Fujita, K. Yamamoto, and M. Tsuji, Controlled van der Waals epitaxy of monolayer MoS_2 triangular domains on graphene, *ACS Appl. Mater. Interfaces* **7**, 5265 (2015).
- [27] H. Li, Q. Zhang, C. C. R. Yap, B. K. Tay, T. H. T. Edwin, A. Olivier, and D. Baillargeat, From bulk to monolayer MoS_2 : Evolution of Raman scattering, *Adv. Funct. Mater.* **22**, 1385 (2012).
- [28] M. Yankowitz, J. Xue, D. Cormode, J. D. Sanchez-Yamagishi, K. Watanabe, T. Taniguchi, P. Jarillo-Herrero, P. Jacquod, and B. J. LeRoy, Emergence of superlattice Dirac points in graphene on hexagonal boron nitride, *Nat. Phys.* **8**, 382 (2012).
- [29] G. Li, A. Luican, J. L. Dos Santos, A. C. Neto, A. Reina, J. Kong, and E. Andrei, Observation of Van Hove singularities in twisted graphene layers, *Nat. Phys.* **6**, 109 (2010).
- [30] X. Liu, I. Balla, H. Bergeron, and M. C. Hersam, Point defects and grain boundaries in rotationally commensurate MoS_2 on epitaxial graphene, *J. Phys. Chem. C* **120**, 20798 (2016).
- [31] K. F. Mak, K. He, C. Lee, G. H. Lee, J. Hone, T. F. Heinz, and J. Shan, Tightly bound trions in monolayer MoS_2 , *Nat. Mater.* **12**, 207 (2013).
- [32] J. Ji, A. Zhang, J. Fan, Y. Li, X. Wang, J. Zhang, E. Plummer, and Q. Zhang, Giant magneto-optical Raman effect in a layered transition metal compound, *Proc. Natl. Acad. Sci. USA* **113**, 2349 (2016).
- [33] W. Jin, P.-C. Yeh, N. Zaki, D. Chenet, G. Arefe, Y. Hao, A. Sala, T. O. Mendes, J. I. Dadap, A. Locatelli, J. Hone, and R. M. Osgood, Jr., Tuning the electronic structure of monolayer graphene/ MoS_2 van der Waals heterostructures via interlayer twist, *Phys. Rev. B* **92**, 201409 (2015).
- [34] C. Zhu, G. Wang, B. Liu, X. Marie, X. Qiao, X. Zhang, X. Wu, H. Fan, P. Tan, T. Amand, and B. Urbaszek, Strain tuning of optical emission energy and polarization in monolayer and bilayer MoS_2 , *Phys. Rev. B* **88**, 121301 (2013).
- [35] A. Zhang, J. Fan, Y. Li, J. Ji, G. Zhao, T. Xia, T. Yan, X. Zhang, W. Zhang, X. Wang, and Q. Zhang, Anomalous valley polarization in monolayer MoSe_2 , [arXiv:1503.08631](https://arxiv.org/abs/1503.08631).
- [36] X. Chen, T. Yan, B. Zhu, S. Yang, and X. Cui, Optical control of spin polarization in monolayer transition metal dichalcogenides, *ACS Nano* **11**, 1581 (2017).
- [37] R. J. Elliott, Theory of the effect of spin-orbit coupling on magnetic resonance in some semiconductors, *Phys. Rev.* **96**, 266 (1954).

- [38] Y. Yafet, Factors and spin-lattice relaxation of conduction electrons, *Solid State Phys.* **14**, 1 (1963).
- [39] M. Dyakonov and V. Perel, Spin relaxation of conduction electrons in noncentrosymmetric semiconductors, *Sov. Phys. Solid State* **13**, 3023 (1972).
- [40] G. L. Bir, A. G. Aronov, and G. E. Pikus, *Zh. Eksp. Teor. Fiz.* **69**, 1382 (1975) [*Sov. Phys. JETP* **42**, 705 (1976)].
- [41] J. Hong, Z. Hu, M. Probert, K. Li, D. Lv, X. Yang, L. Gu, N. Mao, Q. Feng, L. Xie, J. Zhang, D. Wu, Z. Zhang, C. Jin, W. Ji, X. Zhang, J. Yuan, and Z. Zhang, Exploring atomic defects in molybdenum disulphide monolayers, *Nat. Commun.* **6**, 6293 (2015).
- [42] M. Amani, D.-H. Lien, D. Kiriya, J. Xiao, A. Azcatl, J. Noh, S. R. Madhvapathy, R. Addou, S. KC, M. Dubey, K. Cho, R. M. Wallace, S.-C. Lee, J.-H. He, J. W. Ager III, X. Zhang, E. Yablonovitch, and A. Javey, Near-unity photoluminescence quantum yield in MoS₂, *Science* **350**, 1065 (2015).
- [43] L. Cai, J. He, Q. Liu, T. Yao, L. Chen, W. Yan, F. Hu, Y. Jiang, Y. Zhao, T. Hu, Z. Sun, and S. Wei, Vacancy-induced ferromagnetism of MoS₂ nanosheets, *J. Am. Chem. Soc.* **137**, 2622 (2015).
- [44] Y. Zhang, V. W. Brar, C. Girit, A. Zettl, and M. F. Crommie, Origin of spatial charge inhomogeneity in graphene, *Nat. Phys.* **5**, 722 (2009).
- [45] J. Martin, N. Akerman, G. Ulbricht, T. Lohmann, J. v. Smet, K. Von Klitzing, and A. Yacoby, Observation of electron-hole puddles in graphene using a scanning single-electron transistor, *Nat. Phys.* **4**, 144 (2008).
- [46] A. Singh, G. Moody, K. Tran, M. E. Scott, V. Overbeck, G. Berghäuser, J. Schaibley, E. J. Seifert, D. Pleskot, N. M. Gabor, J. Yan, D. G. Mandrus, M. Richter, E. Malic, X. Xu, and X. Li, Trion formation dynamics in monolayer transition metal dichalcogenides, *Phys. Rev. B* **93**, 041401 (2016).
- [47] W. Chen, J. Zhao, J. Zhang, L. Gu, Z. Yang, X. Li, H. Yu, X. Zhu, R. Yang, D. Shi, X. Lin, J. Guo, X. Bai, and G. Zhang, Oxygen-assisted chemical vapor deposition growth of large single-crystal and high-quality monolayer MoS₂, *J. Am. Chem. Soc.* **137**, 15632 (2015).
- [48] H. J. Conley, B. Wang, J. I. Ziegler, R. F. Haglund, Jr., S. T. Pantelides, and K. I. Bolotin, Bandgap engineering of strained monolayer and bilayer MoS₂, *Nano Lett.* **13**, 3626 (2013).
- [49] W. Yang, G. Chen, Z. Shi, C.-C. Liu, L. Zhang, G. Xie, M. Cheng, D. Wang, R. Yang, D. Shi, K. Watanabe, T. Taniguchi, Y. Yao, Y. Zhang, and G. Zhang, Epitaxial growth of single-domain graphene on hexagonal boron nitride, *Nat. Mater.* **12**, 792 (2013).
- [50] D. Pierucci, H. Henck, J. Avila, A. Balan, C. H. Naylor, G. Patriarche, Y. J. Dappe, M. G. Silly, F. Sirotti, A. T. C. Johnson, M. C. Asensio, and A. Ouerghi, Band alignment and minigaps in monolayer MoS₂-graphene van der Waals heterostructures, *Nano Lett.* **16**, 4054 (2016).
- [51] G. Kresse and D. Joubert, From ultrasoft pseudopotentials to the projector augmented-wave method, *Phys. Rev. B* **59**, 1758 (1999).
- [52] G. Kresse and J. Furthmüller, Efficient iterative schemes for ab initio total-energy calculations using a plane-wave basis set, *Phys. Rev. B* **54**, 11169 (1996).
- [53] J. P. Perdew, K. Burke, and M. Ernzerhof, Generalized Gradient Approximation Made Simple, *Phys. Rev. Lett.* **77**, 3865 (1996).